

Galaxy Structure With Strong Gravitational Lensing

Akanksha Katil,¹ Graeme Ko,¹ Michael Jan Klys¹

¹University of Waterloo

Submitted

ABSTRACT

The purpose of this report is to evaluate the structure of galaxies involved in strong gravitational lensing, using the methodology outlined in the paper “Galaxy Structure with Strong Gravitational Lensing: Decomposing the Internal Mass Distribution of Massive Elliptical Galaxies” by James W. Nightingale et al. The methods and results of that paper will be used as a template to perform the analysis for lens galaxy models and source galaxy image reconstruction. The imaging from HST/ACS of selected galaxies from Sloan Lens ACS Survey are fit with the models using PyAutoLens. The light from the lens galaxy is subtracted to reconstruct the surface brightness of the source galaxy. Two independent approaches are chosen for lens modelling, 1)Total Mass model and 2)Decomposed Mass Model. Ultimately, computational limitations made it impossible to enact full searches of all three analyzed galaxies, however partial searches showed good qualitative agreement (where possible) between the reconstructions present in Nightingale et al.’s 2019 paper and our own reconstructions, but with lower Bayesian evidence ([Nightingale et al. \(2019\)](#)) . Future work should extend the use of PyAutolens to novel galaxy structures, and should also focus on increasing the efficiency of modelling physical solutions within PyAutolens pipelines.

Key words: strong lensing – PyAutoLens – galaxy structure

1 INTRODUCTION

Previous work in the field of galaxy structures has shown ray tracing to be an effective methodology for determining the mass and light profiles of structures at high redshifts that are gravitationally lensed around high-mass structures at lower redshifts ([Sonnenfeld et al. \(2013\)](#); [Möller & Blain \(2001\)](#)). In the context of the early universe, gravitational lensing is used to determine the density profiles of early-type galaxies (ETGs) ([Rusin et al. \(2003\)](#)) and stellar initial mass functions ([Treu et al. \(2010\)](#)).

Recently, work has been done towards the creation of an open-source lens modeling software, PyAutolens ([Nightingale et al. \(2019\)](#)). Designed as the first fully automated lensing software requiring minimal user interference in order to create mass-light profiles of systems lensed via strong gravitational lensing ([Nightingale \(2018\)](#)), PyAutolens has been shown to be a powerful tool in the observation of strong-lensing elliptical galaxies ([Smith et al. \(2020\)](#)).

In their 2019 paper, Nightingale et. al demonstrated a use case of PyAutolens, testing models of massive elliptical (ME) galaxy formation through a lens decomposition of their mass and light profiles. This was used to determine their baryonic substructures, as well as the structure of their inner dark matter halos, which in turn was used to determine baryonic accretion and feedback, as well as validating lambda cold dark matter theory([Nightingale et al. \(2019\)](#)).

The goal of this paper is to build on the success of Nightingale et. al in utilising PyAutolens to deconstruct the mass and light profiles of ME systems. Here, the results of the three objects SDSSJ0252, SDSSJ1250, and SDSSJ1430 will be recreated from the Hubble Space Telescope’s Advanced Camera Survey Wide Field Camera. The structure of the paper is as follows. In section 2, we will describe the source of our data sets, as well as the relevant decisions regarding

filters, wavelength and pixel scale, as well as provide a summary of our data reduction. In section 3, we will discuss how we use PyAutolens for strong lens analysis. Section 4 will describe the results of our analysis where we will examine the mass structures of our data sets. Section 5 will feature a discussion on the implications of our results and their significance, as well as consider how future work can build upon the results of this paper. Finally, a summary will be presented in section 6.

2 DATA

The Hubble Space Telescope(HST)’s Advanced Camera Survey(ACS)’s Wide Field Camera(WFC) images are used for the current analysis. The data is taken from MAST:Barbara A. Mikulski Archive for Space Telescopes ([Smith, Collier, Ozaki & Lucey \(MAS\)](#)). The chosen filter is F814W(I-band) to get high resolutions in the IR wavelength. The image from WFC has a pixel scale of 0.05 arcsecond. Table 3 gives the information of the three lensing targets we have chosen for the analysis here. These three lenses are taken from Sloan Lens ACS Survey. The three selected galaxies are Massive Ellipticals(ME)

Deviating from the paper([Nightingale et al. \(2019\)](#)), we work with Charge Transfer Efficiency(CTE) corrected, calibrated, geometrically corrected and dither combined data. The image is first centered on our object of interest and is cropped to a dimension of 74x74 around the centre([fig 1a](#)). The centering is done using the World Coordinate System(WCS). WCS, part of the astropy package, converts pixel coordinates to WCS and vice versa. The right ascension and declination values of the object of interest are used to find the center pixel coordinates.

Table 1. TinyTim Parameters for SLACS1

TinyTim Parameter	Values
Jitter	4
Instrument and Camera	ACS
Detector	WFC1
Position	2194, 1130
Filter	F814W
Spectrum	A07
PSF Diameter	3.0 arcseconds
Focus, secondary mirror despace	-0.776

Once the pixel coordinates of the center are found they are used to produce a Point Spread Function(PSF) using TinyTim(Krist & Hook (1997)). Considered as one of the fundamental image formation step for a telescope, the PSF, describes the imaging system's response(Krist et al. (2011)). The PSF of the HST is very dynamic and depends on a lot of factors including the aperture of the WFC, the focus of the camera, the position on the field of camera and the spectra. To model this dynamic nature of HST a special software TinyTim is developed in C. The PSF is produced at the centre pixel coordinates of the image. The pixel scale of the PSF produced is 0.05 arcseconds.

The focus in table 1 is averaged over the focus model values in the month of October 2006 (Krist, Hook & Stoehr (Foc)). This is because the SLACS1 image was taken on 2 October 2006. The camera specific correction is 0.09 for ACS WFC1(Foc (HST)) is added to the averaged value of focus.

For TinyTim parameters for SLACS2 and SLACS3 see Appendix B.

The mean signal to noise ratio(SNR) of good pixels is stored in the data file(Ryon (2021)). Using the mean SNR value a Poisson distribution is generated. To get the noise in a single pixel the image data value in that pixel are divided by the Poisson distribution value generated in the same pixel(See equation1). The final noise map is shown in fig 1b and the summation of signal and noise is shown in fig 1c.

$$\text{noise} = \frac{\text{image data}}{\text{poisson distribution value}} \quad (1)$$

3 METHODS

3.1 PyAutolens

What follows is a summary description of how PyAutolens deconstructs mass structure, which is described in greater detail in Nightingale et al.'s 2018 paper (Nightingale (2018)). Unlike previous lens modelling attempts, PyAutolens utilises the surface brightness profile of MEs to measure the elliptical's Einstein mass. The mass and light distributions of the lens galaxy are first fitted simultaneously before the surface brightness distribution is placed onto an adaptive pixel grid. A Bayesian framework is then applied in order to determine the most probable mass structure, using a non-linear search algorithm Dynesty, ranking each image and mass reconstruction. Each model image produced by the code is also blurred by the corresponding point spread function, attempting to incorporate the telescope optics into the fit.

Table 3 shows the models used to fit lenses to inputted data. This is used to create a light intensity map that fits the ME, subtracting its

light from the image. A density profile for the lens is generated, from which a deflection angle map is generated, allowing for ray tracing from the image pixels to the plane of the source. The light and mass profiles for the lens galaxy, as well as the source reconstruction, is done simultaneously by PyAutolens, and thus are sampled using the same parameters. Therefore, the profile of the lensing galaxy can be used to generate a stellar density profile as well. Thus, the profile for the source can be fit to both the lens galaxy's light profile as well as the strongly lensed source image. Unlike previous ray-tracing algorithms, this allows us to use two separate assumptions about the mass profile of the lens galaxy; the total-mass model and the decomposed-mass model.

The total-mass model represents both baryonic and dark matter, and the light profile of the lens galaxy is not used to constrain the mass profile. Here, PyAutolens uses the singular isothermal ellipsoid(SIE) as the basis of its mass model for the lens galaxy(density profile of SIE is shown in eq 2). This assumption is most in line with previous work.

$$\kappa_{\text{pl}}(\xi) = \frac{(3 - \alpha)}{1 + q} \left(\frac{\theta_E}{\xi} \right)^{\alpha - 1} \quad (2)$$

where:

θ_E	Einstein Radius
α	Power law density slope = 2
q	axis ratio
ξ	$\xi = \sqrt{x^2 + y^2/q^2}$
(x, y)	center

In the decomposed-mass model, the lens galaxy mass is split into its baryonic and dark matter components, and its light profile is used to determine the baryonic component. In this case, PyAutolens uses either an elliptical Sersic(Eq 3 and surface density profile in eq 4), or a two component Sersic and exponential profile for the baryonic mass profile, and uses a spherical Navarro-Frenk-White profile(Eq 5) for the dark matter component. The advantage of the decomposed mass model is that the light profile is constrained by both the gravitational lensing analysis and the light of the galaxy.

$$I_{\text{Ser}}(\xi_l) = I_l \exp \left\{ -k_l \left[\left(\frac{\xi_l}{R_l} \right)^{\frac{1}{n_l}} - 1 \right] \right\} \quad (3)$$

where:

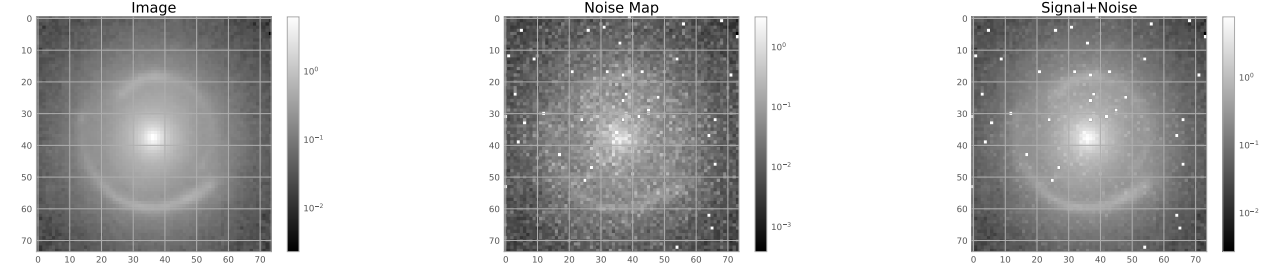
θ_l	Orientation angle
n_l	Sersic Index ($n_l = 1$ for exponential profile)
q_l	Axis ratio
R_l	Effective Radius
I_l	Intensity at Effective Radius
ξ_l	$\xi_l = \sqrt{x_l^2 + y_l^2/q_l^2}$
(x_l, y_l)	center

$$\kappa_{\text{Ser}}(\xi_l) = \Psi_l \left[\frac{q_l \xi_l}{R_l} \right]^{\Gamma_l} I_{\text{Ser}}(\xi_l) \quad (4)$$

where:

Ψ_l	light-to-mass ratio in electrons per second
Γ_l	fold radial dependence into the conversion of mass to light

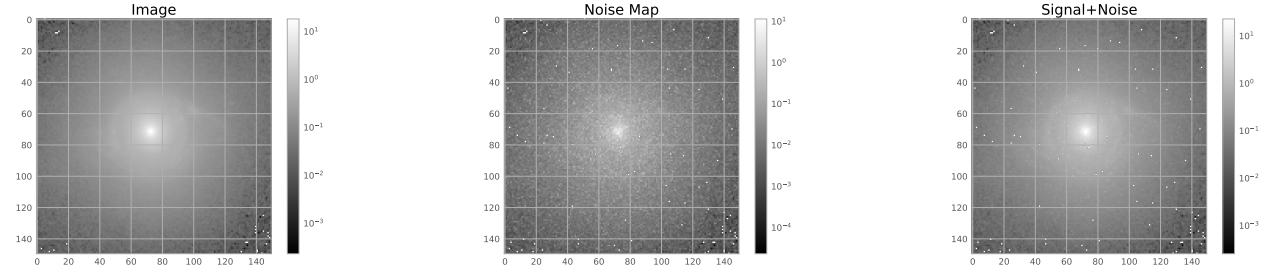
$$\rho = \frac{\rho_s}{(r/r_s)^\gamma (1 + r/r_s)^{3-\gamma}} \quad (5)$$



(a) Cropped Image and centered image

(b) Noise Map

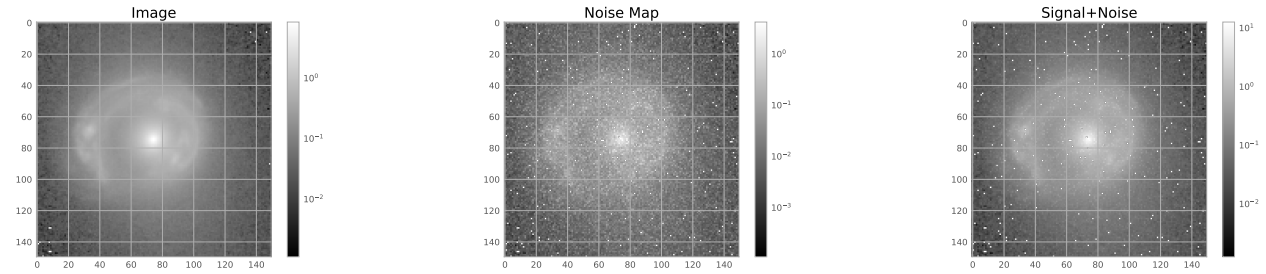
(c) Summing data and noise

Figure 1. SLACS1 Plots

(a) Cropped Image and centered image

(b) Noise Map

(c) Summing data and noise

Figure 2. SLACS2 Plots

(a) Cropped Image and centered image

(b) Noise Map

(c) Summing data and noise

Figure 3. SLACS3 Plots

where:

$$\begin{aligned} \rho_s & \text{ halo normalization} \\ r_s & \text{ scale radius} = 10 R_l \\ \gamma & = 1 \end{aligned}$$

3.2 Lens Fitting Efficiency and Validation

For the purpose of finding the profiles and parameters for the ray tracing models to use, the code takes advantage of a non-linear search algorithm. PyAutoLens has a built-in algorithm called Dynesty which will be used for this paper. However, running a non-linear search directly on the image data requires far too much computation time

given that there are many free parameters to be calculated, especially for complex sources. There are a number of things that will be done to improve efficiency. Masking out the unnecessary pixels that are outside of the lens system helps with this as long as the mask does not interfere too closely with the object pixels. Another method that is used for efficiency are parameter constraints. By constraining parameters such as the Einstein radius, profile centers, and elliptical components to known values or ranges, efficiency is greatly increased and it may promote the finding of global fit solutions instead of local solutions. Parameter constraints are implemented by either setting the parameter to a constant, a range, or a Gaussian centered around the predicted value with an estimated standard deviation. The Gaussian constraints are often the most robust, allowing for predicted

parameters to be efficiently found yet still allow for the possibility of other more accurate solutions. One other control of efficiency is the parameters when the non-linear search is called such as the number of live points to be used during the search. It is also practical to chain non-linear searches such that a very simple model is found first, then the parameters of that model are passed to a series of more precise non-linear searches to make the model more accurate and fit it with more complex profiles. Another neat trick that PyAutoLens can perform is that it takes manually specified co-ordinates of the image plane. When a lens model is fitted it takes these co-ordinates and checks if the fit traces these positions within a specified arc-second threshold of one another in the source-plane.

An example corner plot of parameter space during the non-linear search of the SLACS1 lens can be seen in Figure C1. A corresponding trace plot and parameter convergence behaviour can be seen in Figure C2. This was from a simplified search which is why there were only 12 free parameters to be calculated. The basic model generated from this example fit of SLACS1 did not fit the image well due to its lack of complexity and perhaps ending in a local fit solution and is only meant to give an example of the search.

There is a log-likelihood value and Bayesian evidence value that is output by the non-linear search based on how well the model fits with the given parameters and reduces residuals. The Bayesian evidence value is one of the components that will be used to evaluate the accuracy of the fit and used to compare other models such as the ones in Nightingale et al., 2019 with our own.

3.3 Source Modelling

Source models can be passed to a non-linear search in a similar way to the lens model, and the search will incorporate it into the fit. The most simple sources can be modelled using basic parametric light and mass profiles. However, this is often a poor approximation for sources with complex morphology [Nightingale & Hayes \(Nightingale & Hayes\)](#). Therefore, instead of using parametric source profiles, it is ideal to perform a source inversion where the source pixels in the image plane are mapped back to the source plane while fitting the model, and this source reconstruction will help determine how good the fit is and adjust the model. Most of the pipelines used will begin by fitting the source using a parametric light profile to approximate the lens model, and then pass it to another search where the new lens model will search in conjunction with source inversion to become a more accurate fit assuming the parameters can converge about a solution.

4 RESULTS

4.1 Lens Modelling Remarks

Several built-in (SLaM) and manually written non-linear search pipelines were tried in an attempt to model the lens galaxies. The lenses that were fitted focused on elliptical sersic and elliptical exponential profiles that models the stellar light and mass and a spherical Navarro-Frenk-White profile to model the inner dark halo mass. However, the model fit of these parameter search pipelines were often unable to converge to a solution that gave a high Bayesian evidence value and were very computationally expensive. In an attempt overcome this obstacle, different configurations of prior variables were passed to the non-linear search to reduce the area of parameter space that must be searched through. In many of the model fits, this was still not enough to overcome the computational challenges. Due to

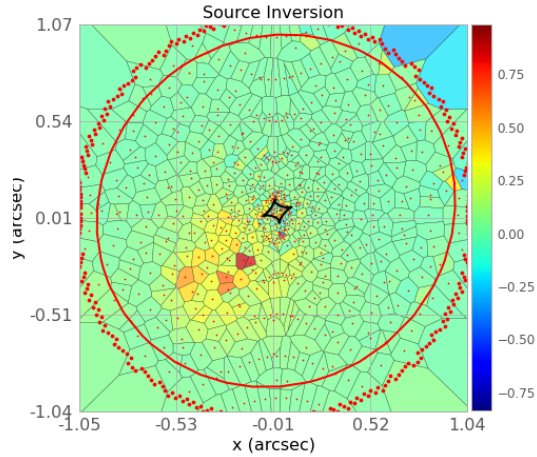


Figure 4. SLACS3 Source reconstruction using Gaussian lens priors

the computational limitations, the analysis did not thoroughly investigate the total mass model, but instead focused on the decomposed model which is expected to give the best fit [Nightingale et al. \(2019\)](#).

4.2 SLACS3 and Direct Ray Tracing

The best fit accomplished had an evidence value of 20313.403, giving parameters of $\kappa = 0.213$ and scale radius = 10.194 for the spherical dark halo profile. The sersic profile had an intensity value of 1.32, effective radius of 0.284, and sersic index of 1.81. The exponential profile had an intensity of 0.110 and effective radius of 6.06.

Source galaxy reconstruction was attempted in a non-linear search pipeline and also through direct ray-tracing using the lens galaxy parameters found by Nightingale et al. [Nightingale et al. \(2019\)](#).

Figure 4 shows a source reconstruction using a Voronoi tessellation grid output by a search pipeline where all SLACS3 lens parameters except shear were given as Gaussian priors based on the parameters found in the reference paper model and the static pixelization and regularization source components were not given prior parameters. The evidence value was only around -52000 and the lens model was unable to converge to a solution. This gives a poor model of the caustic which can be seen when comparing Figure 4 to the corresponding reconstruction in the reference paper, though despite the inaccurate lens model, the source reconstruction seems to visually share some key features when comparing the relative locations of bright pixels and some of the extended morphology. It also seems to have incorporated noise into reconstruction, which may be attenuated by using an adaptive grid instead that adjusts the reconstruction to a pixel weight map based on the noise map. The source reconstruction found by Nightingale et al. can be seen in Figure 6

Source reconstruction was also attempted using a non-linear search pipeline without any prior parameters that begins by modelling the source using simple profiles to model the lens and system, and then passes the arguments to another non-linear search where the source inversion occurs using the non-adaptive Voronoi tessellation grid. The highest evidence search for this pipeline gave a value of approximately 19500, though it was likely a local solution and the model deteriorated in further searches where the dark mass profile was adjusted. The resulting source reconstruction can be seen in Figure 5

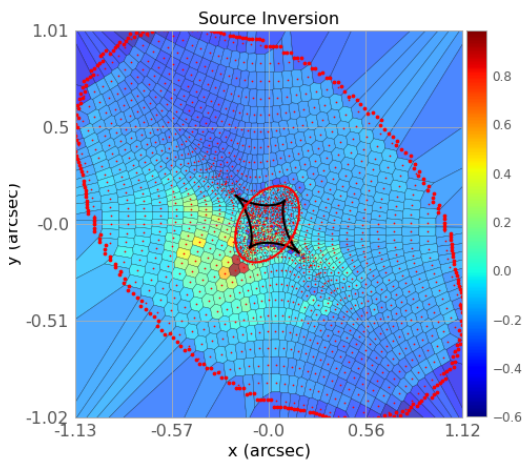


Figure 5. SLACS3 Source reconstruction using a chained search without priors

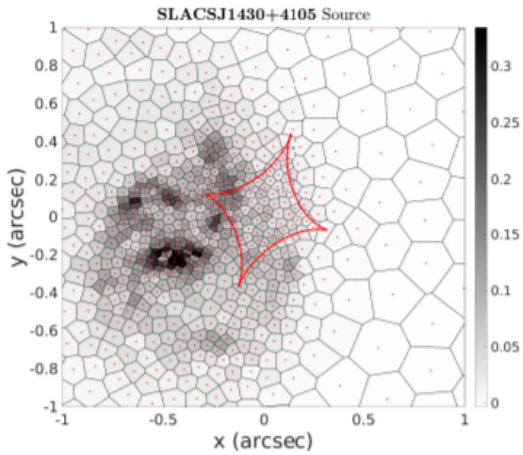


Figure 6. SLACS3 Source reconstruction taken from [Nightingale et al. \(2019\)](#)

which visually shows somewhat similar behaviour in terms of the location of bright pixels, yet lacks fidelity in the extended structures.

Direct ray-tracing of SLACS1 and SLACS3 using the given lens model showed source reconstructions very similar in shape to the overall original image, which may imply that the solutions are under-magnified as described in the paper 'Auto-identification of unphysical source reconstructions in strong gravitational lensing' [Maresca et al. \(2021\)](#) which looks at correcting these types of solutions with Convolutional Neural Networks. Using static pixelization saw similar results to using pixelization which adapts to the source brightness to avoid unnecessary calculation of noise pixels. The static pixelization gave an evidence value of 16672.661 for SLACS3 reconstruction, whereas the adaptive pixelization gave an evidence value of 17116.097. Note that these evidence values depend on input parameters, which for the direct ray tracing was set to constants and would be subject to change in a non-linear search to attempt to find even higher evidence values. Furthermore, the shear profile of the lens galaxy was not included in this analysis as the shear parameters were not specified in the model solutions of [Nightingale et al.'s paper](#).

4.3 SLACS1

The SLaM(Source, Light and Mass) pipelines are used to fit complex models. The motivation behind using SLaM pipelines was to fit a decomposed lens model. The lens and source bulge is modeled using sersic model, whereas the lens disk is modeled using exponential sersic. The total mass and dark matter are modeled using SIE and spherical NFW respectively. The fit could not go past the third search pipeline, which was simultaneously fitting the lens galaxy's bulge, lens galaxy's disk, total mass distribution, source galaxy's bulge and external shear, a total of 23 parameters. See table 4 for the maximum likelihood model.

As seen in fig 8 there is still structure observed in the residual map. This is expected as the fit hasn't converged.

The complexity of the non linear search is reduced to produce a less computationally intensive fit model. First the lens disk(Exponential Sersic) and bulge(Sersic) are fitted. The results from this non-linear search are then used to model the dark matter mass distribution(Spherical NFW), external shear and source galaxy's light(Sersic). These results are used for source reconstruction with the VoronoiMagnification pixelizations of source galaxy's light.

Figure 9 is still almost like fig 8. The source construction for the fit is shown in fig 10

Comparing fig 11a and fig 11b it is clear the source reconstruction from the simplified pipeline is not the best.

There are several pipelines used for fitting and source reconstruction of SLACS1 but due to time constraints only SLaM and simplified pipelines gave substantial results.

4.4 SLACS2

Figure 9 shows the source reconstruction found in [Nightingale et al.'s 2019 paper](#) in comparison to the source reconstruction done using SLaM pipeline and further methodologies discussed above [Nightingale et al. \(2019\)](#). Due to limits in computational power, the reconstruction is not based off of a full array of searches, but rather is produced solely by the first inversion search. Despite this, the calculated Bayesian evidence value of this model remains quite high at 23530. However, this value still falls a full order of magnitude below those achieved by [Nightingale et al. Nightingale et al. \(2019\)](#). What follows is a qualitative analysis and comparison of the general structure and substructures present within each reconstruction.

There exists relatively good agreement between the two images in regard to the general structure of the galaxy. Both exhibit a narrow horizontal structure reducing in intensity away from the center of the image. There exists within the structure two significant substructures present in each reconstruction. The first is a concentration located just above the center of the image. The second obvious substructure is an area of increased intensity towards the right of the central band, separated by a relative void of inactivity from the core of the structure. There also exists, in general, larger amounts of activity above the central band in each image than below. Finally, quantitatively, there is generalized agreement in regards to the size and proportions of the structure and substructures. Each image shows a central structure approximately 0.5 arcseconds across, with the right most substructure approximately 0.3 arcseconds away from this central structure. Thus we see that, despite varying in Bayesian evidence by an order of magnitude, there still exists some agreement between the two images.

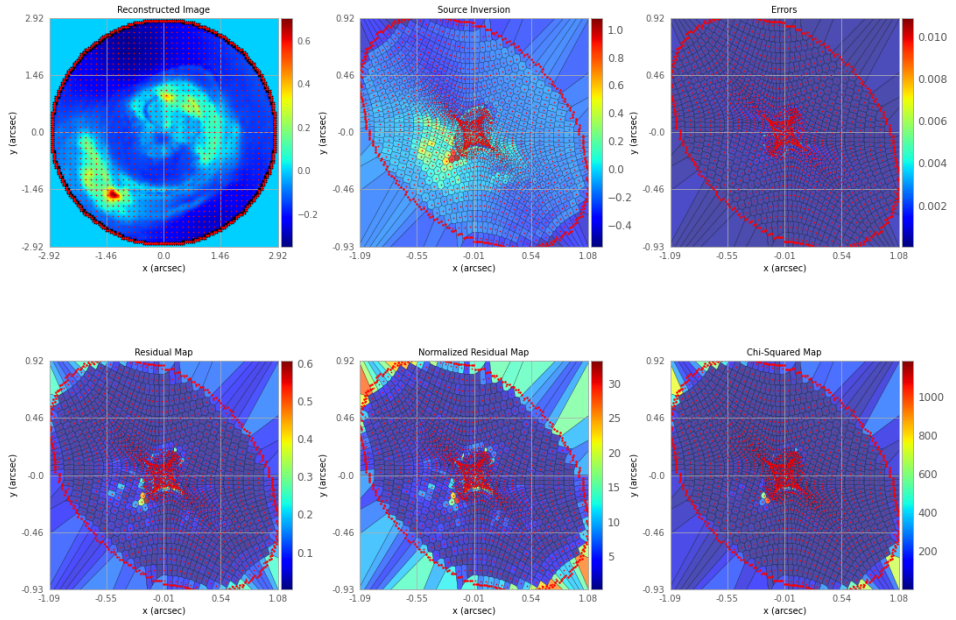


Figure 7. SLACS3 Source reconstruction subplot

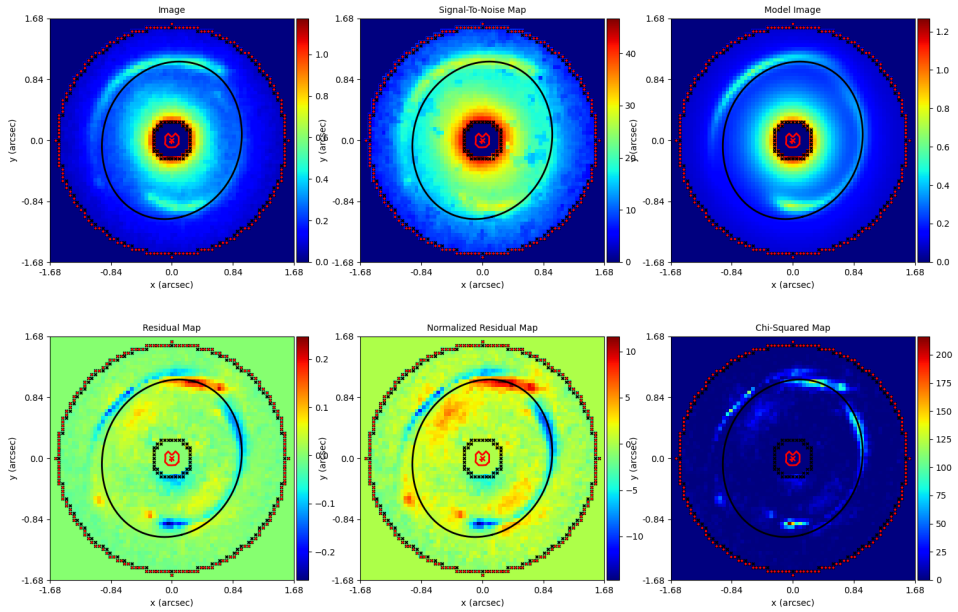


Figure 8. Residual Map for SLACS1 fit with SLAM output

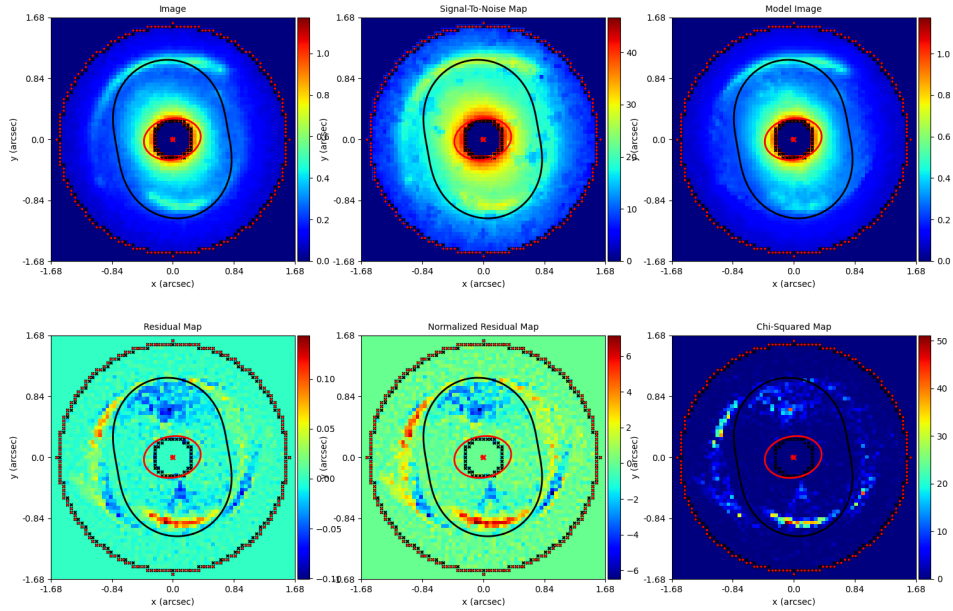


Figure 9. Residual Map for SLACS1 fit with Simplified output

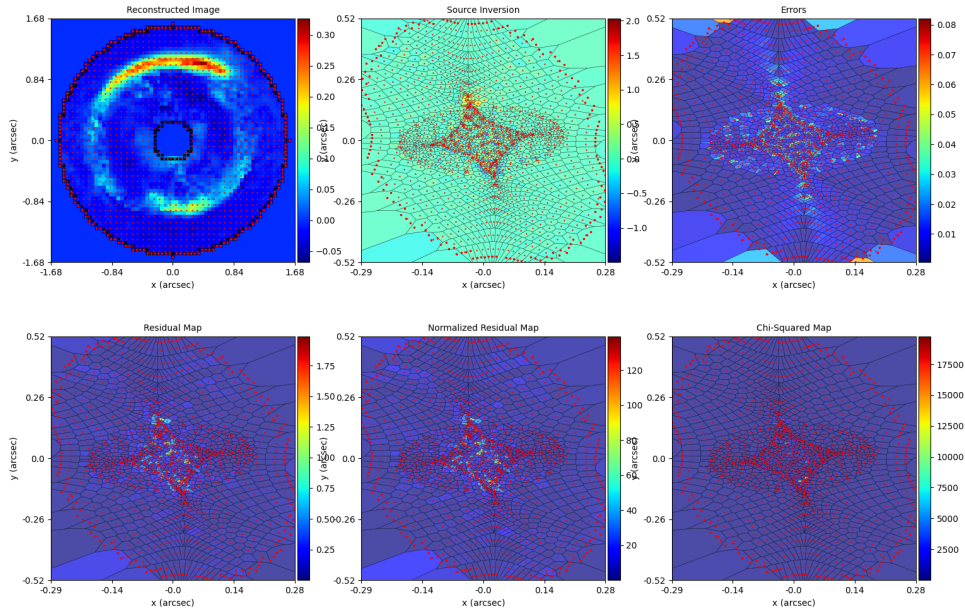


Figure 10. Source reconstruction of SLACS1 using a simplified pipeline

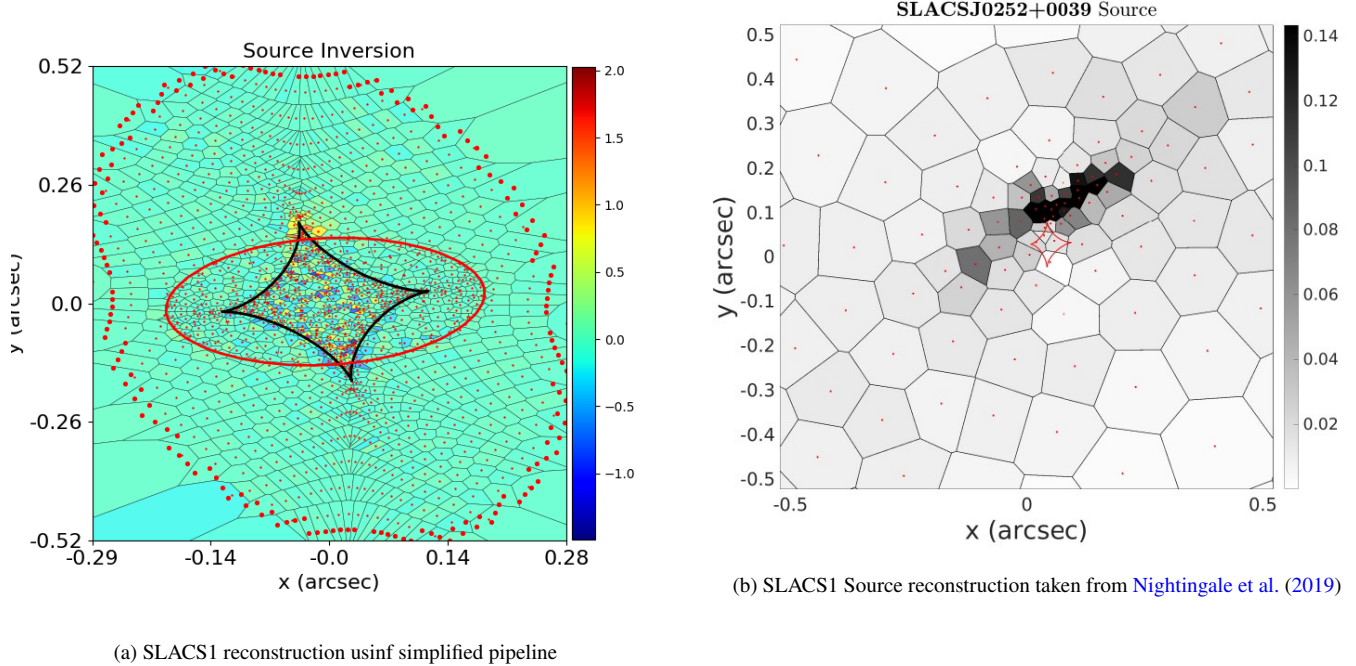


Figure 11. SLACS1 Reconstruction

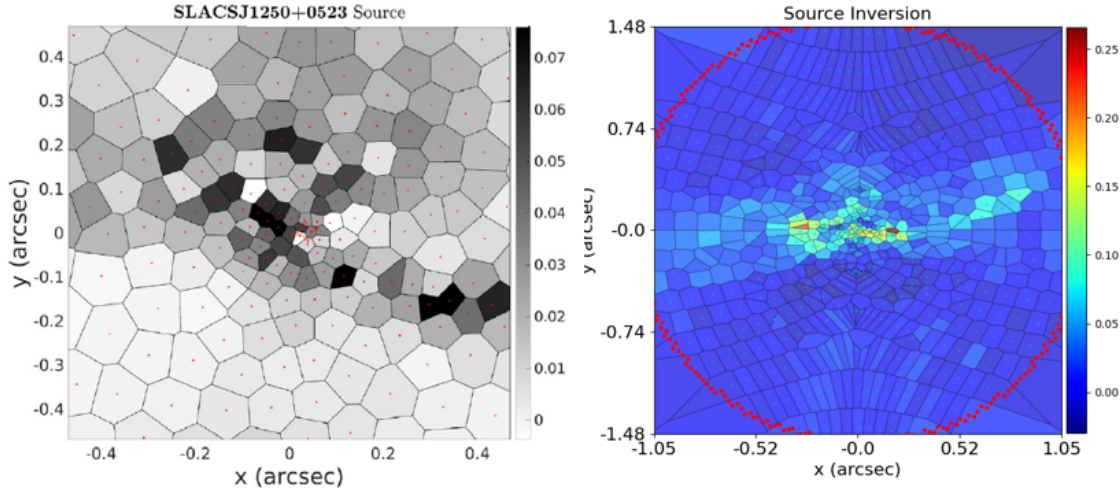


Figure 12. Left: SLACS2 source reconstruction. Taken from [Nightingale et al. \(2019\)](#). Right: SLACS2 source reconstruction using SLaM pipeline.

5 DISCUSSION

5.1 Considerations of Bayesian Evidence when Using Source Inversions

Bayesian evidence favours simpler fits over complex fits during source conversion. This is because it assumes the noise will follow a Gaussian pattern in the residuals of a good model fit, otherwise it is likely that inversion has over-fitted the model. Therefore the number of pixels needed for the fit and regularization value which determines the level of pixel smoothing in the source inversion will impact the Bayesian evidence of the fit [Nightingale & Hayes \(Nightingale & Hayes\)](#). The direct ray tracing that was tested did not find the regularization and pixelization parameters through a non-linear search

and was instead set manually, and therefore the Bayesian evidence for the ray tracing fits may be higher for adjusted parameters. This also shows that the Bayesian evidence value depends on more factors than just the chi-squared residuals.

5.2 Complexity and Comparing Models

We did not expect to get a perfect lens model as the decomposed mass model of an elliptical sersic + exponential stellar light and mass profile and spherical Navarro-Frenk-White dark mass profile are still not enough to fully model complex systems without error [Nightingale et al. \(2019\)](#). However, there was a distinct difference between the Bayesian evidence of our models and the evidence given

in Nightingale et al.'s paper, where the highest evidence we achieved was on the scale of 10^4 and the evidence achieved in the paper was on the scale of 10^5 for many different models. While the Bayesian evidence depends on many factors and model choices and not just on the chi-squared residuals, this discrepancy is still quite significant. An evidence value on the scale of 10^4 seems to be rather high in general considering the examples given in the PyAutoLens documentation which tend to be described as having a somewhat good fit on the scale of 10^3 [Nightingale & Hayes](#) ([Nightingale & Hayes](#)), though still very small compared to the values found in the reference paper.

Perhaps their analysis performed better image processing before the non-linear searches, such as choosing different masking values than us which could influence the amount of noise involved in the fitting or also allow more valuable lens or source pixels to be included. The masking apertures we used were circular shaped, but perhaps they masked their data using a custom shape that contoured the image pixels better. It is also assumed that the generated PSF will account for the telescope optics, but maybe their analysis had a more rigorous optics correction than ours.

Another major difference could be the prior constraints they used for their models. Depending on which priors they used, they may have been able to restrict the parameter space of the model fit closer to a global solution than we were able to. Furthermore, if the priors we used in some of the models were too strict, then this may have had a negative impact on the ability for the non-linear search to search through high evidence solutions. The searches that had many priors corresponding the model found in the paper should have theoretically been close to similar solutions, though we were not able to find appropriate shear values to use for the mass profile priors.

6 CONCLUSION

The purpose of this report was to evaluate PyAutolens, an open source fully-automated lensing software, as a tool for reconstructing lensed gravitational structures, with the goal of recreating the results found by Nightingale et al. in their 2019 paper 'Galaxy structure with strong gravitational lensing: decomposing the internal mass distribution of massive elliptical galaxies' [Nightingale et al. \(2019\)](#). To this end, three lens galaxies evaluated by Nightingale et al. were chosen, and scripts where created using PyAutolens search chaining, ray tracing, and SLaM pipelines in order to find the resulting structures and compare it to the model fit in their original paper. Despite improving software efficiency wherever possible, computational limitations caused a failure to enact full non-linear searches for all three galaxies. Regardless, partial searches resulted in relatively high Bayesian evidence values of 6203 for SLACS1, 23530 for SLACS2, and 20313 for SLACS3, with evidence values an order of magnitude less of those found in the original 2019 paper ([Nightingale et al. \(2019\)](#)). Where qualitative comparison was possible, it was found that even an incomplete search could produce structures that shared visual similarity with those reported by Nightingale et al. Ultimately, we concluded that PyAutolens is a useful tool for analysing strong gravitational lensing, with room for experimentation in order to increase efficiency of searches. Further research should extend the use of PyAutolens to novel galactic lensing images using more powerful computational tools, and should also focus on increasing the parameter search adaptability and efficiency of the software for this application.

REFERENCES

- Focus Model Values for the year 2006, https://www.stsci.edu/files/live/sites/www/files/home/hst/instrumentation/focus-and-pointing/focus/hst-focus-model/_documents/Focus2006.txt
- HST Focus Model, <https://www.stsci.edu/hst/instrumentation/focus-and-pointing/focus/hst-focus-model>
- Krist J., Hook R., 1997, The Tiny Tim User's Guide
- Krist J. E., Hook R. N., Stoehr F., 2011, in Optical Modeling and Performance Predictions V. p. 81270J
- MAST:Barbara A. Mikulski Archive for Space Telescopes, <https://mast.stsci.edu/portal/Mashup/Clients/Mast/Portal.html>
- Maresca J., Dye S., Li N., 2021, Monthly Notices of the Royal Astronomical Society, 503, 2229
- Möller O., Blain A., 2001, Monthly Notices of the Royal Astronomical Society, 327, 339
- Nightingale S. Dye R. M., 2018, Monthly Notices of the Royal Astronomical Society, 478, 4738
- Nightingale J., Hayes R., , PyAutoLens - Read the Docs, <https://pyautolens.readthedocs.io/en/latest/index.html>
- Nightingale J. W., Massey R. J., Harvey D. R., Cooper A. P., Etherington A., Tam S.-I., Hayes R. G., 2019, Monthly Notices of the Royal Astronomical Society, 489, 2049
- Rusin D., et al., 2003, The Astrophysical Journal, 587, 143
- Ryon J., 2021, ACS Instrument Handbook for Cycle 29 v. 20.0, 20, 20
- Smith R. J., Collier W. P., Ozaki S., Lucey J. R., 2020, Monthly Notices of the Royal Astronomical Society: Letters, 493, L33
- Sonnenfeld A., Gavazzi R., Suyu S. H., Treu T., Marshall P. J., 2013, The Astrophysical Journal, 777, 97
- Treu T., Auger M. W., Koopmans L. V., Gavazzi R., Marshall P. J., Bolton A. S., 2010, The Astrophysical Journal, 709, 1195

]

Table 2. Properties of SLACS lenses. Taken from [Nightingale et al. \(2019\)](#)

Target name	RA	Dec	z_{lens}	z_{src}	σ_{SDSS} (km/s)	Near a cluster?
SDSSJ0252+0039 (SLACS1)	02 h 52'45.21"	+00°39'58"	0.2803	0.9818	164 ±12	
SDSSJ1250+0523 (SLACS2)	12 h 50'28.26"	+05°23'49"	0.2318	0.7953	252 ±14	
SDSSJ1430+4105 (SLACS3)	14 h 30'04.10"	+41°05'57"	0.2850	0.5753	322 ±32	MaxBCGJ217.49493+41.10435 (z=0.270)

]

Table 3. Light and mass models available to PyAutoLens in order to model strong lenses. Taken from [Nightingale et al. \(2019\)](#)

Model	Components	Represents
Sersic	Light+Mass	Stellar Matter
Exponential	-	-
Singular Isothermal Ellipsoid	Mass	Total(Stellar+Dark Matter)
Singular Isothermal Sphere	-	-
Spherical NFW	-	Dark Matter
Elliptical NFW	-	-
Generalized Spherical NFW	-	-
Shear	-	Line of Sight

[]

Table 4. SLACS1 SLAM Pipeline Max Log Likelihood model

Maximum Log Likelihood	Lens Bulge Elliptical Components	Lens Bulge Intensity	Lens Bulge Effective Radius	Lens Bulge Sersic Index	Lens Disk Elliptical Components
2907.46	(-0.008, -0.038)	2907.45873695	2.705	4.937	(-0.079, -0.305)
Lens Disk Intensity	Lens Disk Effective Radius	Lens Disk and Bulge Center	Total Mass Einstein Radius	Total Mass Elliptical Components	External Shear Elliptical Components
0.000	7.309	(-0.016, -0.007)	1.028	(0.087, -0.073)	(0.042, -0.015)
Source Bulge Elliptical Components	Source Bulge Intensity	Source Bulge Effective Radius	Source Bulge Effective Radius	Source Bulge Center	
(0.500, -0.134)	0.376	0.051	1.044	(0.087, -0.027)	

[]

Table 5. SLACS1 Simplified Pipeline Max Log Likelihood model

Maximum Log Likelihood	Lens Bulge Elliptical Components	Lens Bulge Intensity	Lens Bulge Effective Radius	Lens Bulge Sersic Index	Lens Disk Elliptical Components
6203.36482827	(0.026, 0.026)	1.763	0.133	0.801	(-0.039, -0.084)
Lens Disk Intensity	Lens Disk Effective Radius	Lens Disk and Bulge Center	Dark Kappa s	Dark Scale Radius	External Shear Elliptical Components
0.206	1.035	(0.003, -0.008)	0.249	5.433	(0.028, 0.075)
Source Bulge Elliptical Components	Source Bulge Intensity	Source Bulge Effective Radius	Source Bulge Sersic Index	Source Bulge Center	
(0.091, -0.019)	0.243	0.025	0.804	(0.170, -0.026)	

Table B1. TinyTim Parameters for SLACS2

TinyTim Parameter	Values
Jitter	4
Instrument and Camera	ACS
Detector	WFC1
Position	2190, 1129
Filter	F814W
Spectrum	A07
PSF Diameter	3.0 arcseconds
Focus, secondary mirror despace	-0.776

Table B2. TinyTim Parameters for SLACS3

TinyTim Parameter	Values
Jitter	4
Instrument and Camera	ACS
Detector	WFC1
Position	2192, 1134
Filter	F814W
Spectrum	A07
PSF Diameter	3.0 arcseconds
Focus, secondary mirror despace	-0.776

APPENDIX A: DATA REDUCTION CODE

The data reduction class in python is developed so that it takes the image data from HST/ACS, right ascension and declination of the object of interest as input and yields the centered cropped data with noise map, PSF and convolution.

The code is in [GitHub](#)

APPENDIX B: TINYTIM PARAMETER TABLES

The following are parameters used for TinyTim for SLACS2 and SLACS3 respectively.

APPENDIX C: NON-LINEAR SEARCH PARAMETER SPACE PLOTS

This paper has been typeset from a $\text{\TeX}/\text{\LaTeX}$ file prepared by the author.

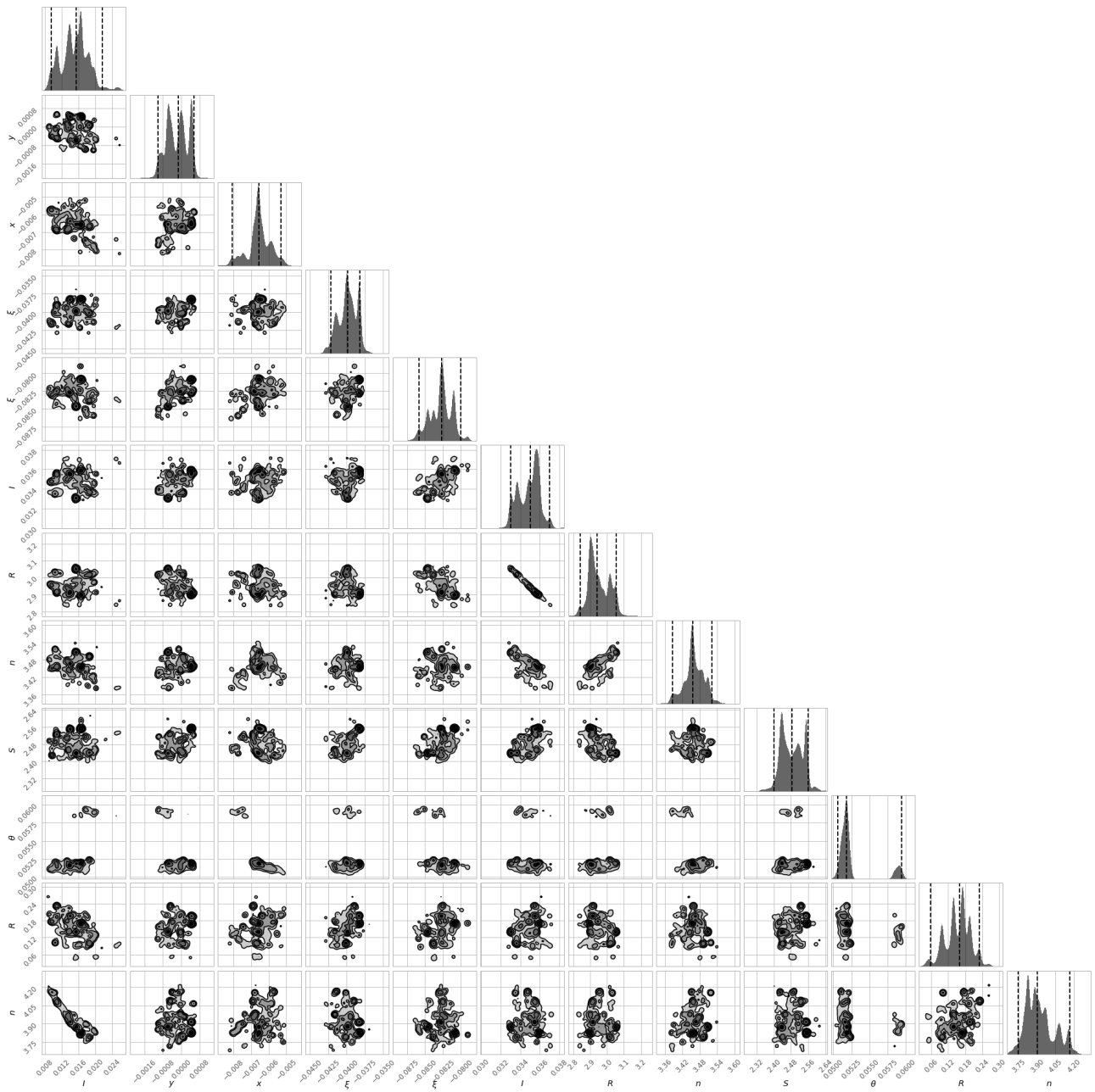


Figure C1. Example Parameter Search Corner Plot

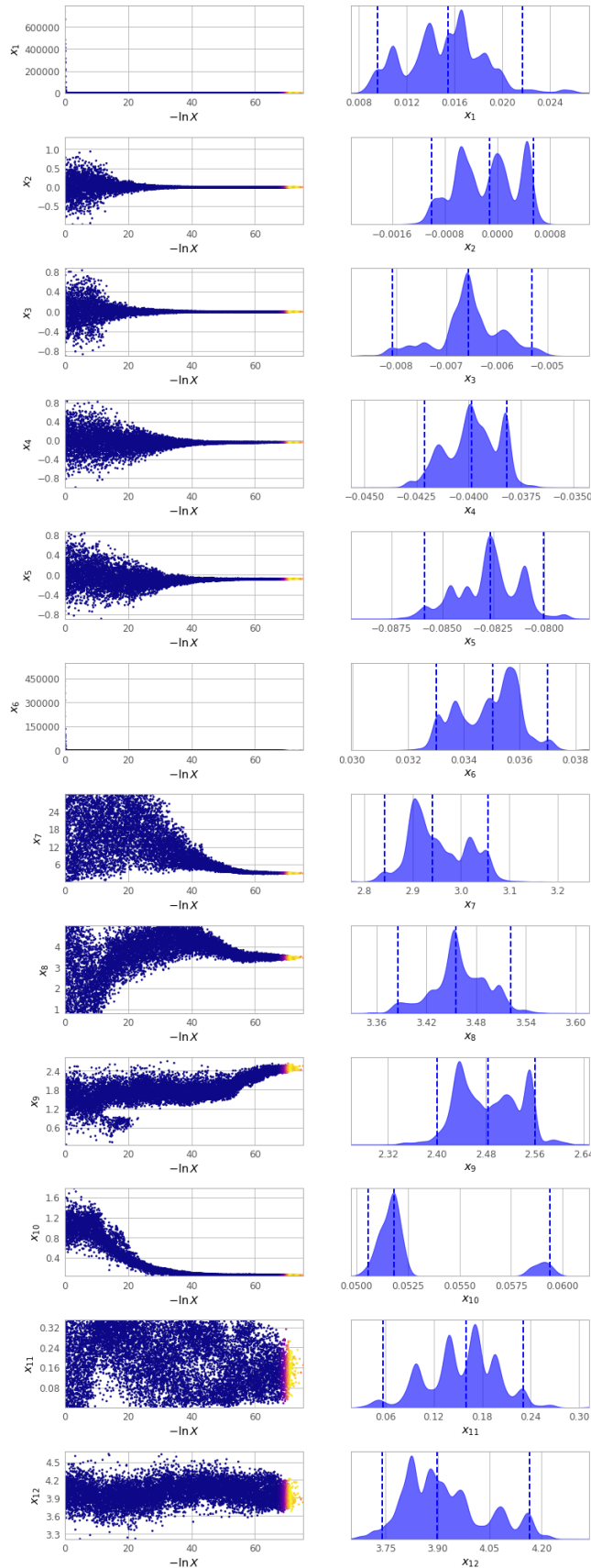


Figure C2. Example Parameter Search Trace Plot